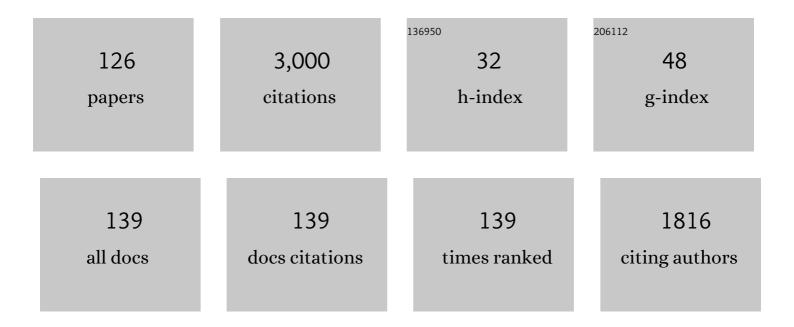
Jörg Matysik

List of Publications by Year in descending order

Source: https://exaly.com/author-pdf/6128409/publications.pdf Version: 2024-02-01



#	Article	IF	CITATIONS
1	Photo-CIDNP in Solid State. Applied Magnetic Resonance, 2022, 53, 521-537.	1.2	11
2	Low Carbon Footprint Recycling of Post onsumer PET Plastic with a Metagenomic Polyester Hydrolase. ChemSusChem, 2022, 15, .	6.8	70
3	An integrated systems-level model of the toxicity of brevetoxin based on high-resolution magic-angle spinning nuclear magnetic resonance (HRMAS NMR) metabolic profiling of zebrafish embryos. Science of the Total Environment, 2022, 803, 149858.	8.0	11
4	Longâ€Term Preservation of Short‣ived Photoproducts of Phytochromes at Room Temperature. ChemPhotoChem, 2022, 6, .	3.0	3
5	Gold(<scp>i</scp>) complexes of tetra- <i>tert</i> -butylcyclotetraphosphane. Dalton Transactions, 2022, 51, 4627-4633.	3.3	3
6	Solid-state NMR and hyperpolarization methods for the Research, Development, and Innovation in Costa Rican science. Biophysical Reviews, 2022, 14, 549-551.	3.2	3
7	Light- and pH-dependent structural changes in cyanobacteriochrome AnPixJg2. Photochemical and Photobiological Sciences, 2022, 21, 447-469.	2.9	6
8	An integrated systems-level model of ochratoxin A toxicity in the zebrafish (Danio rerio) embryo based on NMR metabolic profiling. Scientific Reports, 2022, 12, 6341.	3.3	5
9	Timeâ€Dependent Hydrogen Bond Network Formation in Glycerolâ€Based Deep Eutectic Solvents. ChemPhysChem, 2022, 23, e202100806.	2.1	4
10	Timeâ€Dependent Hydrogen Bond Network Formation in Glycerolâ€Based Deep Eutectic Solvents. ChemPhysChem, 2022, 23, e202200283.	2.1	2
11	Spectroscopic insight into post-synthetic surface modification of porous glass beads as a silica model system. Physical Chemistry Chemical Physics, 2022, 24, 14488-14497.	2.8	2
12	Mapping the role of aromatic amino acids within a blue-light sensing LOV domain. Physical Chemistry Chemical Physics, 2021, 23, 16767-16775.	2.8	7
13	Mechanistic investigation of enzymatic degradation of polyethylene terephthalate by nuclear magnetic resonance. Methods in Enzymology, 2021, 648, 231-252.	1.0	11
14	Hydrogen Bond between a Tyrosine Residue and the <i>C</i> -Ring Propionate Has a Direct Influence on Conformation and Absorption of the Bilin Cofactor in Red/Green Cyanobacteriochromes. Journal of Physical Chemistry B, 2021, 125, 1331-1342.	2.6	5
15	Theoretical Assessment of Hinge-Type Models for Electron Donors in Reaction Centers of Photosystems I and II as well as of Purple Bacteria. Journal of Physical Chemistry B, 2021, 125, 3066-3079.	2.6	6
16	Flow MAS NMR for In Situ Monitoring of Carbon Dioxide Capture and Hydrogenation Using Nanoporous Solids. Journal of Physical Chemistry C, 2021, 125, 10219-10225.	3.1	5
17	Metabolic Profiling of Suprachiasmatic Nucleus Reveals Multifaceted Effects in an Alzheimer's Disease Mouse Model. Journal of Alzheimer's Disease, 2021, 81, 797-808.	2.6	2
18	Introduction to a special issue of <i>Magnetic Resonance</i> in honour of Robert Kaptein at the occasion of his 80th birthday. Magnetic Resonance, 2021, 2, 465-474.	1.9	0

#	Article	IF	CITATIONS
19	Metabolomic and transcriptomic profiling of adult mice and larval zebrafish leptin mutants reveal a common pattern of changes in metabolites and signaling pathways. Cell and Bioscience, 2021, 11, 126.	4.8	4
20	The relation between crystal structure and the occurrence of quantum-rotor-induced polarization. Magnetic Resonance, 2021, 2, 751-763.	1.9	4
21	In situ synthesis and characterization of sulfonic acid functionalized hierarchical silica monoliths. Journal of Sol-Gel Science and Technology, 2020, 96, 67-82.	2.4	3
22	Lyophilization Reveals a Multitude of Structural Conformations in the Chromophore of a Cph2-like Phytochrome. Journal of Physical Chemistry B, 2020, 124, 7115-7127.	2.6	5
23	Selective functionalization of the outer surface of MCM-48-type mesoporous silica nanoparticles at room temperature. Journal of Nanoparticle Research, 2020, 22, 1.	1.9	11
24	Tailored flavoproteins acting as light-driven spin machines pump nuclear hyperpolarization. Scientific Reports, 2020, 10, 18658.	3.3	12
25	Comparative toxicometabolomics of perfluorooctanoic acid (PFOA) and next-generation perfluoroalkyl substances. Environmental Pollution, 2020, 265, 114928.	7.5	58
26	Inverse Vulcanization of Styrylethyltrimethoxysilane–Coated Surfaces, Particles, and Crosslinked Materials. Angewandte Chemie - International Edition, 2020, 59, 18639-18645.	13.8	33
27	UV Pretreatment Impairs the Enzymatic Degradation of Polyethylene Terephthalate. Frontiers in Microbiology, 2020, 11, 689.	3.5	46
28	Analysis of the electronic structure of the primary electron donor of photosystemÂl of <i>Spirodela oligorrhiza</i> by photochemically induced dynamic nuclear polarization (photo-CIDNP) solid-state nuclear magnetic resonance (NMR). Magnetic Resonance, 2020, 1, 261-274.	1.9	6
29	Same spectral signature in liquid-state and solid-state ¹ H photo-CIDNP NMR spectra of cyclohexanone. Molecular Physics, 2019, 117, 2756-2761.	1.7	2
30	Studying hydrogen bonding and dynamics of the acetylate groups of the Special Pair of Rhodobacter sphaeroides WT. Scientific Reports, 2019, 9, 10528.	3.3	3
31	Degeneration of the Suprachiasmatic Nucleus in an Alzheimer's Disease Mouse Model Monitored by in vivo Magnetic Resonance Relaxation Measurements and Immunohistochemistry. Journal of Alzheimer's Disease, 2019, 69, 363-375.	2.6	14
32	Synthesis of highly active ETS-10-based titanosilicate for heterogeneously catalyzed transesterification of triglycerides. Beilstein Journal of Nanotechnology, 2019, 10, 2039-2061.	2.8	2
33	Biocatalytic Degradation Efficiency of Postconsumer Polyethylene Terephthalate Packaging Determined by Their Polymer Microstructures. Advanced Science, 2019, 6, 1900491.	11.2	181
34	NMR-Based Metabolic Profiles of Intact Zebrafish Embryos Exposed to Aflatoxin B1 Recapitulates Hepatotoxicity and Supports Possible Neurotoxicity. Toxins, 2019, 11, 258.	3.4	41
35	Accessing the First <i>nido</i> arborane‣ubstituted Diphosphetane: A Ligand and Synthon for <i>nido</i> arboranylphosphanes. Chemistry - A European Journal, 2019, 25, 11456-11465.	3.3	7
36	15N–1H Transfer of Light-Induced Nuclear Hyperpolarization in Frozen Photosynthetic Reaction Centers. Applied Magnetic Resonance, 2019, 50, 695-708.	1.2	4

#	Article	IF	CITATIONS
37	Magnetic field and orientation dependence of solid-state CIDNP. Journal of Chemical Physics, 2019, 150, 094105.	3.0	11
38	15N photo-CIDNP MAS NMR analysis of a bacterial photosynthetic reaction center of Rhodobacter sphaeroides wildtype. Journal of Chemical Physics, 2019, 151, 195101.	3.0	8
39	Nuclear spin-hyperpolarization generated in a flavoprotein under illumination: experimental field-dependence and theoretical level crossing analysis. Scientific Reports, 2019, 9, 18436.	3.3	14
40	Conformational fitting of a flexible oligomeric substrate does not explain the enzymatic PET degradation. Nature Communications, 2019, 10, 5581.	12.8	89
41	15N photo-CIDNP MAS NMR on both photosystems and magnetic field-dependent 13C photo-CIDNP MAS NMR in photosystem II of the diatom Phaeodactylum tricornutum. Photosynthesis Research, 2019, 140, 151-171.	2.9	13
42	Assignment of NMR resonances of protons covalently bound to photochemically active cofactors in photosynthetic reaction centers by 13C–1H photo-CIDNP MAS-J-HMQC experiment. Journal of Magnetic Resonance, 2019, 298, 64-76.	2.1	3
43	Simple device for dissolution and sample transfer for applications in spin-hyperpolarizationÂ. Molecular Physics, 2019, 117, 2772-2776.	1.7	4
44	Spectroscopic Properties of Lumiflavin: A Quantum Chemical Study. Photochemistry and Photobiology, 2019, 95, 662-674.	2.5	15
45	15N photo-CIDNP MAS NMR analysis of reaction centers of Chloracidobacterium thermophilum. Photosynthesis Research, 2018, 137, 295-305.	2.9	20
46	Analysis of the Electronic Structure of the Special Pair of a Bacterial Photosynthetic Reaction Center by ¹³ C Photochemically Induced Dynamic Nuclear Polarization Magicâ€Angle Spinning <scp>NMR</scp> Using a Doubleâ€Quantum Axis. Photochemistry and Photobiology, 2018, 94, 69-80.	2.5	8
47	Sex- and age-specific modulation of brain GABA levels in a mouse model of Alzheimer's disease. Neurobiology of Aging, 2018, 62, 168-179.	3.1	38
48	Photochemically induced dynamic nuclear polarization NMR on photosystem II: donor cofactor observed in entire plant. Scientific Reports, 2018, 8, 17853.	3.3	16
49	3D Structures of Plant Phytochrome A as Pr and Pfr From Solid-State NMR: Implications for Molecular Function. Frontiers in Plant Science, 2018, 9, 498.	3.6	32
50	13C → 1H transfer of light-induced hyperpolarization allows for selective detection of protons in frozen photosynthetic reaction center. Journal of Magnetic Resonance, 2018, 293, 82-91.	2.1	11
51	The Flavin–Tryptophan Dyad F10T as a Cryptochrome Model Compound: Synthesis and Photochemistry. ChemPhotoChem, 2017, 1, 12-16.	3.0	8
52	Photo-CIDNP in the Reaction Center of the Diatom <i>Cyclotella meneghiniana</i> Observed by ¹³ C MAS NMR. Zeitschrift Fur Physikalische Chemie, 2017, 231, 347-367.	2.8	15
53	In Situ and in Operando Characterization of Mixing Dynamics in Liquidâ€Phase Reactions by ¹²⁹ Xe NMR Spectroscopy. ChemPhysChem, 2017, 18, 1513-1516.	2.1	1
54	Crystal Effects on Mesobilirubin: A Combined NMR Spectroscopic and Density Functional Theory Study. Photochemistry and Photobiology, 2017, 93, 834-843.	2.5	0

#	Article	IF	CITATIONS
55	Penta- and hexaorganostannate(iv) complexes based on O-heterocyclic ligands. Dalton Transactions, 2017, 46, 8279-8285.	3.3	11
56	Structural heterogeneity in a parent ground-state structure of AnPixJg2 revealed by theory and spectroscopy. Physical Chemistry Chemical Physics, 2017, 19, 13882-13894.	2.8	21
57	Introduction, Festschrift in honor of Wolfgang Gätner. Photochemistry and Photobiology, 2017, 93, 640-641.	2.5	0
58	Field-cycling NMR with high-resolution detection under magic-angle spinning: determination of field-window for nuclear hyperpolarization in a photosynthetic reaction center. Scientific Reports, 2017, 7, 12111.	3.3	15
59	Magnetic field effect in natural cryptochrome explored with model compound. Scientific Reports, 2017, 7, 11892.	3.3	11
60	Pseudomorphic Transformation of Porous Glasses into Micelleâ€Templated Silica. Chemie-Ingenieur-Technik, 2017, 89, 863-875.	0.8	8
61	Rational development of Stafib-2: a selective, nanomolar inhibitor of the transcription factor STAT5b. Scientific Reports, 2017, 7, 819.	3.3	34
62	Metabolic profiling of zebrafish (Danio rerio) embryos by NMR spectroscopy reveals multifaceted toxicity of l²-methylamino-L-alanine (BMAA). Scientific Reports, 2017, 7, 17305.	3.3	35
63	Level crossing analysis of chemically induced dynamic nuclear polarization: Towards a common description of liquid-state and solid-state cases. Journal of Chemical Physics, 2016, 144, 144202.	3.0	35
64	Dynamic Nuclear Polarization Provides New Insights into Chromophore Structure in Phytochrome Photoreceptors. Angewandte Chemie, 2016, 128, 16251-16254.	2.0	2
65	Dynamic Nuclear Polarization Provides New Insights into Chromophore Structure in Phytochrome Photoreceptors. Angewandte Chemie - International Edition, 2016, 55, 16017-16020.	13.8	22
66	High-Resolution Magic Angle Spinning Nuclear Magnetic Resonance of Intact Zebrafish Embryos Detects Metabolic Changes Following Exposure to Teratogenic Polymethoxyalkenes from Algae. Zebrafish, 2016, 13, 456-465.	1.1	17
67	Effect of pretreatment temperature on the surface modification of diatomite with trimethylchlorosilane. Journal of Porous Materials, 2016, 23, 1439-1449.	2.6	13
68	Chapter 9. Probing Exchange and Diffusion in Confined Systems by 129Xe NMR Spectroscopy. New Developments in NMR, 2016, , 294-317.	0.1	5
69	The Solid-State Photo-CIDNP Effect. Wuli Huaxue Xuebao/ Acta Physico - Chimica Sinica, 2016, 32, 399-404.	4.9	3
70	A Red/Green Cyanobacteriochrome Sustains Its Color Despite a Change in the Bilin Chromophore's Protonation State. Biochemistry, 2015, 54, 5839-5848.	2.5	44
71	NMR chemical shift pattern changed by ammonium sulfate precipitation in cyanobacterial phytochrome Cph1. Frontiers in Molecular Biosciences, 2015, 2, 42.	3.5	5
72	Color Tuning in Red/Green Cyanobacteriochrome AnPixJ: Photoisomerization at C15 Causes an Excited-State Destabilization. Journal of Physical Chemistry B, 2015, 119, 9688-9695.	2.6	32

#	Article	IF	CITATIONS
73	Photochemically Induced Dynamic Nuclear Polarization Observed by Solid-State NMR in a Uniformly ¹³ C-Isotope-Labeled Photosynthetic Reaction Center. Journal of Physical Chemistry B, 2015, 119, 13897-13903.	2.6	6
74	The D-ring, Not the A-ring, Rotates in Synechococcus OS-B′ Phytochrome*. Journal of Biological Chemistry, 2014, 289, 2552-2562.	3.4	46
75	Spectral editing through laser-flash excitation in two-dimensional photo-CIDNP MAS NMR experiments. Journal of Magnetic Resonance, 2014, 246, 9-17.	2.1	12
76	Spin in Photosynthetic Electron Transport. , 2014, , 141-170.		9
77	The field-dependence of the solid-state photo-CIDNP effect in two states of heliobacterial reaction centers. Photosynthesis Research, 2013, 117, 461-469.	2.9	8
78	Bacteriopheophytin <i>a</i> in the Active Branch of the Reaction Center of <i>Rhodobacter sphaeroides</i> Is Not Disturbed by the Protein Matrix as Shown by ¹³ C Photo-CIDNP MAS NMR. Journal of Physical Chemistry B, 2013, 117, 3287-3297.	2.6	8
79	Symmetry Break of Special Pair: Photochemically Induced Dynamic Nuclear Polarization NMR Confirms Control by Nonaromatic Substituents. Journal of the American Chemical Society, 2013, 135, 10382-10387.	13.7	16
80	Solid‣tate <scp>NMR</scp> Spectroscopy to Probe Photoactivation in Canonical Phytochromes. Photochemistry and Photobiology, 2013, 89, 259-273.	2.5	40
81	The Solid-State Photo-CIDNP Effect and Its Analytical Application. Topics in Current Chemistry, 2012, 338, 105-121.	4.0	21
82	Whole Cell Nuclear Magnetic Resonance Characterization of Two Photochemically Active States of the Photosynthetic Reaction Center in Heliobacteria. Biochemistry, 2012, 51, 5763-5773.	2.5	19
83	Electron Spin Density Distribution in the Special Pair Triplet of <i>Rhodobacter sphaeroides</i> R26 Revealed by Magnetic Field Dependence of the Solid-State Photo-CIDNP Effect. Journal of the American Chemical Society, 2012, 134, 5921-5930.	13.7	46
84	Solid-State NMR Spectroscopic Study of Chromophore–Protein Interactions in the Pr Ground State of Plant Phytochrome A. Molecular Plant, 2012, 5, 698-715.	8.3	30
85	Exploring Chromophore-Binding Pocket: High-Resolution Solid-State 1H–13C Interfacial Correlation NMR Spectra with Windowed PMLG Scheme. Applied Magnetic Resonance, 2012, 42, 79-88.	1.2	7
86	15N Photo-CIDNP MAS NMR To Reveal Functional Heterogeneity in Electron Donor of Different Plant Organisms. Applied Magnetic Resonance, 2012, 42, 57-67.	1.2	17
87	Spin Chemistry: Coherent Spin Dynamics Rules Chemical Reactions. Applied Magnetic Resonance, 2012, 42, 1-3.	1.2	3
88	On the Collective Nature of Phytochrome Photoactivation. Biochemistry, 2011, 50, 10987-10989.	2.5	21
89	Theory of Solid-State Photo-CIDNP in the Earth's Magnetic Field. Journal of Physical Chemistry A, 2011, 115, 9919-9928.	2.5	21
90	A 10 000-fold Nuclear Hyperpolarization of a Membrane Protein in the Liquid Phase via a Solid-State Mechanism. Journal of the American Chemical Society, 2011, 133, 16754-16757.	13.7	31

#	Article	IF	CITATIONS
91	Solvation and Crystal Effects in Bilirubin Studied by NMR Spectroscopy and Density Functional Theory. Journal of Physical Chemistry A, 2011, 115, 11696-11714.	2.5	10
92	Two ground state isoforms and a chromophore <i> D </i> -ring photoflip triggering extensive intramolecular changes in a canonical phytochrome. Proceedings of the National Academy of Sciences of the United States of America, 2011, 108, 3842-3847.	7.1	161
93	Nanosecond-Flash 15N Photo-CIDNP MAS NMR on Reaction Centers of Rhodobacter sphaeroides R26. Applied Magnetic Resonance, 2010, 37, 49-63.	1.2	13
94	Action Spectroscopy on Dense Samples of Photosynthetic Reaction Centers of Rhodobacter sphaeroides WT Based on Nanosecond Laser-Flash 13C Photo-CIDNP MAS NMR. Applied Magnetic Resonance, 2010, 38, 105-116.	1.2	1
95	Observation of the solid-state photo-CIDNP effect in entire cells of cyanobacteria Synechocystis. Photosynthesis Research, 2010, 104, 275-282.	2.9	38
96	Role of the Protein Cavity in Phytochrome Chromoprotein Assembly and Doubleâ€bond Isomerization: A Comparison with Model Compounds. Photochemistry and Photobiology, 2010, 86, 856-861.	2.5	14
97	Hyperpolarization Methods and Applications in NMR. , 2010, , 963-970.		7
98	Phytochrome as Molecular Machine: Revealing Chromophore Action during the Pfr → Pr Photoconversion by Magic-Angle Spinning NMR Spectroscopy. Journal of the American Chemical Society, 2010, 132, 4431-4437.	13.7	55
99	Solid-State Photo-CIDNP Effect Observed in Phototropin LOV1-C57S by ¹³ C Magic-Angle Spinning NMR Spectroscopy. Journal of the American Chemical Society, 2010, 132, 15542-15543.	13.7	51
100	The electronic structure of the primary electron donor of reaction centers of purple bacteria at atomic resolution as observed by photo-CIDNP ¹³ C NMR. Proceedings of the National Academy of Sciences of the United States of America, 2009, 106, 22281-22286.	7.1	74
101	The solid-state photo-CIDNP effect. Photosynthesis Research, 2009, 102, 427-435.	2.9	54
102	Differential Charge Polarization of Axial Histidines in Bacterial Reaction Centers Balances the Asymmetry of the Special Pair. Journal of the American Chemical Society, 2009, 131, 9626-9627.	13.7	20
103	Electronâ^'Nuclear Spin Dynamics in a Bacterial Photosynthetic Reaction Center. Journal of Physical Chemistry C, 2009, 113, 10269-10278.	3.1	42
104	Photo-CIDNP MAS NMR beyond the T1 limit by fast cycles of polarization extinction and polarization generation. Journal of Magnetic Resonance, 2008, 190, 43-51.	2.1	22
105	Characterization of the Primary Radical Pair in Reaction Centers of <i>Heliobacillus mobilis</i> by ¹³ C Photo-CIDNP MAS NMR. Biochemistry, 2008, 47, 4629-4635.	2.5	33
106	Reply to Hengge: On the 31P chemical shifts of the phosphorane compounds : Fig. 1 Proceedings of the National Academy of Sciences of the United States of America, 2008, 105, E85-E85.	7.1	2
107	Light-induced chromophore activity and signal transduction in phytochromes observed by ¹³ C and ¹⁵ N magic-angle spinning NMR. Proceedings of the National Academy of Sciences of the United States of America, 2008, 105, 15229-15234.	7.1	85
108	13C Photo-CIDNP MAS NMR on the LH1-RC Complex of Rhodopseudomonas acidophila. , 2008, , 55-58.		4

13C Photo-CIDNP MAS NMR on the LH1-RC Complex of Rhodopseudomonas acidophila. , 2008, , 55-58. 108

#	Article	IF	CITATIONS
109	Photochemically Induced Dynamic Nuclear Polarization (Photo-CIDNP) Magic-Angle Spinning NMR. Advances in Photosynthesis and Respiration, 2008, , 385-399.	1.0	32
110	¹⁵ N photochemically induced dynamic nuclear polarization magic-angle spinning NMR analysis of the electron donor of photosystem II. Proceedings of the National Academy of Sciences of the United States of America, 2007, 104, 12767-12771.	7.1	64
111	Signals in Solid-State Photochemically Induced Dynamic Nuclear Polarization Recover Faster Than Signals Obtained with the Longitudinal Relaxation Time. Journal of Physical Chemistry B, 2007, 111, 10606-10614.	2.6	28
112	¹³ C Chemical Shift Map of the Active Cofactors in Photosynthetic Reaction Centers of <i>Rhodobacter sphaeroides</i> Revealed by Photo-CIDNP MAS NMR. Biochemistry, 2007, 46, 8953-8960.	2.5	33
113	Photochemically induced dynamic nuclear polarization in the reaction center of the green sulphur bacterium Chlorobium tepidum observed by 13C MAS NMR. Biochimica Et Biophysica Acta - Bioenergetics, 2007, 1767, 610-615.	1.0	26
114	Photo-CIDNP MAS NMR in Intact Cells ofRhodobactersphaeroidesR26:Â Molecular and Atomic Resolution at Nanomolar Concentration. Journal of the American Chemical Society, 2006, 128, 12794-12799.	13.7	56
115	15N MAS NMR Studies of Cph1 Phytochrome:Â Chromophore Dynamics and Intramolecular Signal Transduction. Journal of Physical Chemistry B, 2006, 110, 20580-20585.	2.6	51
116	Photo-CIDNP solid-state NMR on Photosystems I and II:what makes P680 special?. Photosynthesis Research, 2005, 84, 303-308.	2.9	32
117	Magnetic Field Dependence of Photo-CIDNP MAS NMR on Photosynthetic Reaction Centers ofRhodobacter sphaeroidesWT. Journal of the American Chemical Society, 2005, 127, 14290-14298.	13.7	67
118	Heteronuclear 2D (1H-13C) MAS NMR Resolves the Electronic Structure of Coordinated Histidines in Light-Harvesting Complex II: Assessment of Charge Transfer and Electronic Delocalization Effect. Journal of Biomolecular NMR, 2004, 28, 157-164.	2.8	18
119	Photochemically Induced Dynamic Nuclear Polarization in Photosystem I of Plants Observed by13C Magic-Angle Spinning NMR. Journal of the American Chemical Society, 2004, 126, 12819-12826.	13.7	58
120	Photochemically induced dynamic nuclear polarisation in entire bacterial photosynthetic units observed by 13C magic-angle spinning NMR. Journal of Molecular Structure, 2003, 661-662, 625-633.	3.6	9
121	Probing the electronic structure of tyrosine radical YD in photosystem II by EPR spectroscopy using site specific isotope labelling in Spirodela oligorrhiza. Chemical Physics, 2003, 294, 459-469.	1.9	13
122	13C MAS NMR and Photo-CIDNP Reveal a Pronounced Asymmetry in the Electronic Ground State of the Special Pair of Rhodobacter sphaeroides Reaction Centers. Biochemistry, 2002, 41, 8708-8717.	2.5	59
123	Ultrahigh Field MAS NMR Dipolar Correlation Spectroscopy of the Histidine Residues in Light-Harvesting Complex II from Photosynthetic Bacteria Reveals Partial Internal Charge Transfer in the B850/His Complex. Journal of the American Chemical Society, 2001, 123, 4803-4809.	13.7	56
124	Photo-CIDNP 13C Magic Angle Spinning NMR on Bacterial Reaction Centres: Exploring the Electronic Structure of the Special Pair and Its Surroundings. Biological Chemistry, 2001, 382, 1271-1276.	2.5	20
125	Fourier-Transform Resonance Raman Spectroscopy of Intermediates of the Phytochrome Photocycle. Biochemistry, 1995, 34, 10497-10507.	2.5	109
126	A spectroscopic insight of the porous structure of hydrophobic silica aerogels by hyperpolarized 129Xe NMR. Journal of Sol-Gel Science and Technology, 0, , 1.	2.4	6